Accepted for 14th International Detonation Symposium,
April 11-16, 2010, Coeur d'Alene, Idaho

From Intermolecular Shearing to Composite Behavioral Predictions for Initiation of Energetic Materials

Ronald W. Armstrong* and Wayne L. Elban[f]

*Center for Energetic Concepts Development
Department of Mechanical Engineering
University of Maryland, College Park, MD 20742, U.S.A.

[f]Department of Engineering
Loyola University Maryland, Baltimore, MD 21210

Abstract. Hardness measurements for energetic and reference inert crystals are assessed on a dislocation mechanics basis. The dislocation pile-up avalanche model for hot spot development is applied to explanation of crystal size dependencies in drop-weight impact, particle compaction, combustion, and shock experiments. Shock sensitivity measurements for energetic materials show an added complication of initiation pressures being generally higher than those required for phase transformations in the solid state.

Introduction

The potential brittleness of solid energetic materials, whether in the form of individual crystals or as ingredients within a heavily-filled, plastic-bonded explosive (PBX), has led to hardness testing as a useful method of determining the role of plastic flow, particularly in the form of dislocation pile-ups, in causing consequent cracking and fracturing.[1] The hardness applications have been greatly enhanced by the use of nano-indentation testing methods and analyses. And, for a number of energetic and reference inert crystals, the occurrence of localized heating that results from obstacle-cracking release of pile-ups, then as concentrated dislocation avalanches, provides connection with the "hot spot" model historically established as a necessary requirement for the initiation of explosive decompositions.[2]

In the present report, key measurements and model evaluations are developed consistent with the foregoing hot spot mechanism to include: (1) verification of relatively higher (hardness-determined) strength levels being exhibited normally by crystals of high explosives; (2) elucidation of the dislocation pile-up mechanism of crack formation and temperature-rise-associated avalanching; (3) predicted crystal size dependence determined in drop-weight impact sensitivity experiments, also, involving predictive Arrhenius-type constitutive equation behavior; and, (4) extension to similar crystal size dependencies for particle compaction, combustion, and composite material shock results, with associated concerns for contiguous particle contacts and inter-particle porosities. Of special note at the greater strain rates produced in shock and isentropic compression tests of energetic and related materials is the additional complication shown of the operative pressures being greater than those required for phase transformations in the solid state.

Elastic, plastic, cracking behaviors

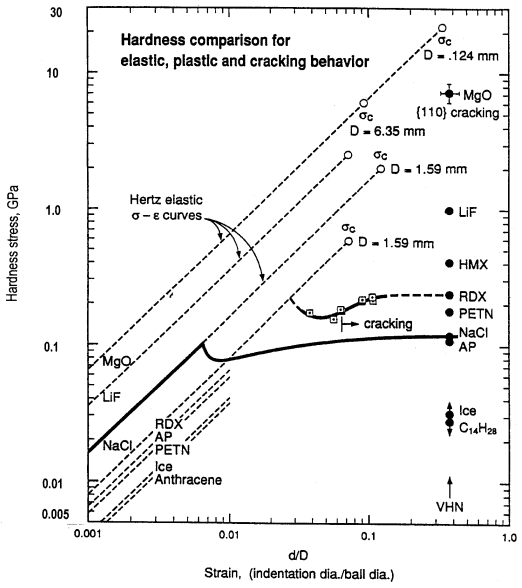

Fig. 1. Stress – strain curves for energetic and inert crystals based on a continuous indentation test.

In Fig. 1, the hardness stress, σ_H, is the applied load divided by the projected circular area of contact, or its equivalent; and, the strain is the equivalent contact diameter, d, divide by the ball diameter, D. At (d/D) = 0.375 are plotted the Vickers hardness numbers (VHN's) determined for a number of crystals.[1]

The linear Hertz elastic lines follow the equation

$$\sigma_H = \frac{4}{3\pi}\left(\frac{1-\nu_S^{\,2}}{E_S}+\frac{1-\nu_B^{\,2}}{E_B}\right)^{-1}(d/D) \qquad (1)$$

In eq. (1), ν_S, E_S and ν_B, E_B are the Poisson's ratio and Young's modulus for the specimen and ball, respectively. The hardness cracking stresses, σ_C, are shown on the elastic loading lines in accordance with the indentation fracture mechanics (IFM) equation

$$\sigma_C = \left(\frac{4E_S\gamma}{\pi D\left(1-\nu_S^{\,2}\right)\left(\kappa_1^{\,2}+\kappa_2^{\,2}\right)}\right)^{1/2}(d/D)^{-1/2} \qquad (2)$$

In eq. (2), γ is the crack surface energy and $(\kappa_1^{\,2} + \kappa_2^{\,2}) = 2 \times 10^{-5}$. The top-most D value associated with σ_C for MgO is determined as an equivalent value for the average VHN measurement; and, the effect of increasing D on lowering σ_C is shown at the marked $D = 6.35$ mm value.[3]

Of importance in Fig. 1 is a comparison of the shown hardness measurements for RDX and the continuous stress - strain curve and confirming VHN measurement for NaCl. The lower Hertzian curve for RDX shows its molecular bonding to be elastically more compliant, as expected, but the higher RDX hardness is a result of difficult dislocation shear displacements across interleaved molecules within the orthorhombic crystal lattice.[4] And, the lower σ_C of RDX at the same $D = 1.59$ mm value is indicative of easier cracking. Thus RDX, typical of high explosive molecular crystals, is shown to be elastically soft, plastically hard, and brittle. Also, the smaller increase from σ_H to σ_C for RDX is indicative of a smaller range in stress being available for dynamic loading. The consideration relates to the correlation of hardness and impact sensitivity measurements.

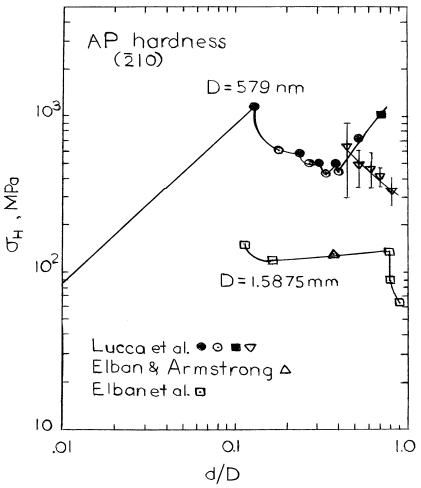

Fig. 2. Hardness stress – strain results for AP.[5-7]

Another comparison is shown in Fig. 2, this time, of continuous loading curves determined in nano- and macro-indentation tests performed on AP (oxidizer) crystals; see in Fig.1 the VHN point for AP. In Fig. 2, the upper nano-indentation

curve has been obtained through use being made of the Berkovich indenter having a rounded tip. A value of D = 579 nm was determined for the initial Hertzian dependence of load, P, on elastic penetration depth, h_e, in accordance with the relation

$$D = (9/8)P^2 E_R^{-2} h_e^{-3} \quad (3)$$

In eq. (3), a value of E_R = 20.5 GPa applies for the reciprocal bracketed factor in Eq. (1). The linear Hertzian dependence was computed with $d_e = \sqrt{(2h_eD)}$ in the evaluation of (d_e/D) and σ_e.

At (d_e/D) = (0.13) in Fig. 2, a maximum elastic contact stress of σ_e = 1.14 GPa was obtained for (h_{e0}, P) = (5 nm, 5.2 μN), the point of first "pop-in" of plastic deformation. The next open circle point on the stress – strain curve was obtained at the same constant load value but now by obtainment of a larger $d_P = 2\sqrt{\{([h_{e0}/\sqrt{2}] + \Delta h_P)(D - h_t)\}}$ in which $\Delta h_P = h_t - h_{e0}$ and h_t is the total penetration depth. The following pop-in (filled and open circle) points were computed on the basis of taking $\Delta h_P = \Delta h_t$. At the crossed overlapping sharp rise in plastic hardness points and downward pointing triangle points, the hardness computations are somewhat uncertain because of the indenter shape transition from a spherical tip to the designed triangular pyramid.

In Fig. 2, the typically higher nanoindentation curve is attributed to the indenter sampling a locally defect-free crystal volume. The lower macroscopic loading curve shown for D = 1.5875 mm is matched with the upward pointing triangle point for a VHN measurement.[6,7] In this case, the elastic loading deformation is seen to be negligible and there is agreement with the micro-indentation hardness measurement. The sharp drop in stress at (d/D) ~ 0.8 was caused by cracking.

Figure 3 is shown for dislocation model connection with hardness indentations spanning the nano-, micro-, and macro-scales. A Vickers impression is shown for an (001) MgO crystal surface in which the indentation alignment matches nicely with the operative slip and cracking systems. Indentation-forming screw dislocation pile-ups are shown to spread first along the <100> directions and produce troughs in the raised picture-framed surroundings that, in turn,

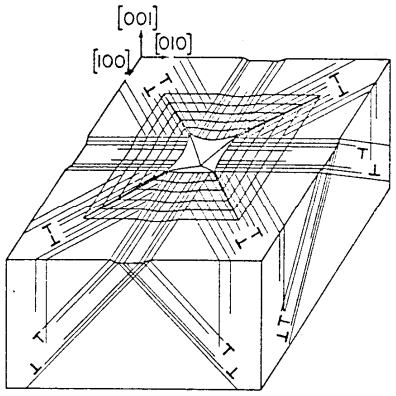

Fig. 3. Dislocation {110}<110> slip displacements produced at an aligned Vickers hardness indent made on a cleaved (001) MgO crystal surface.

require stress concentrations from intersecting dislocation pile-ups along diagonal internal <111> directions to produce cleavage cracking on the difficult vertically-standing {110} planes.[1,8] The described dislocation and cracking mechanisms, that were primarily worked-out from dislocation etch pitting and x-ray topography results, have been analogously demonstrated to apply also for indentations made on AP and RDX crystals.[6, 9]

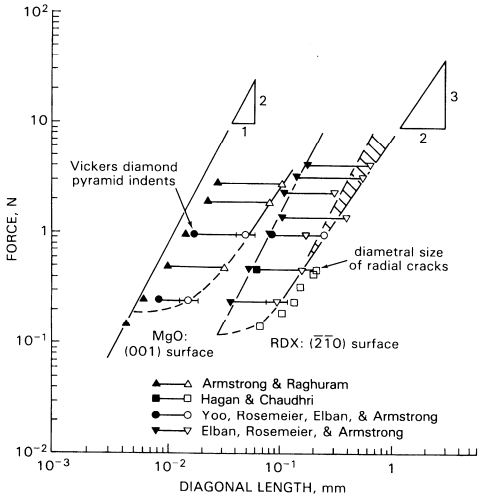

Fig. 4. Hardness and IFM crack size measurements for Vickers-indented MgO and RDX crystals.[10-13]

Figure 4 shows a comparison of MgO and RDX cracking results as determined on an IFM basis in which the tip-to-tip diagonal crack lengths should follow a log/log (3/2) dependence while a constant hardness would follow a 2.0 dependence.[13] The results have been interpreted to show that MgO is substantially weakened by pile-up induced cracking while RDX needs less stress concentration because of its intrinsic brittleness.

Dislocation mechanics

Lattice-dependent dislocation modeling has been performed for a [100] slip direction on (040) and (02-1) slip planes in RDX and for [10-1](101) twinning in HMX.[4] On such basis, dislocation movement was shown to be difficult consistent with reported experimental measurements. The intermolecular blockages to dislocation shear in RDX have been related to nitroso-compound reactions detected in drop-weight impact tests under near-initiation condition. Heterogeneous nucleation of dislocations on the listed RDX slip planes has been reported for molecular dynamics model calculations of a Rankine-Hugoniot-defined shock pressure of ~1.5 GPa applied to [111]-oriented crystals, and to be followed by homogeneous nucleation of dislocations on (001) planes at a pressure of ~1.8 GPa. [14] At an even higher pressure of 9.7 GPa applied in an [001] direction onto an (100) oriented crystal, the occurrence of shear banding was found to occur at 45° to [100] in the [010] zone. The results are of interest here because the α-RDX to γ-RDX phase transformation occurs at ~3.8 GPa at ambient temperature and the α-RDX to β-RDX occurs at the same pressure at ~225°C.[15]

Whereas the relative difficulty of dislocation movement is established for energetic crystals, not unlike the somewhat differently explained case for many ceramic materials, an assessment of the extent of localized heating that can be generated by deformation was shown to require the concerted action of multiple dislocations, as for cracking, and even then, the movement must occur rapidly.[2] Figure 5 shows a schematic model description whereby both temperature rise requirements are met.

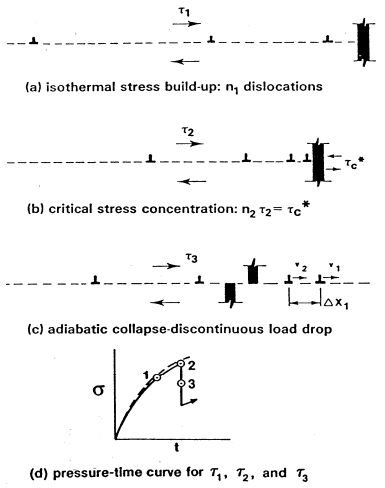

Fig.5. Schematic pile-up formation and avalanche.

In Fig. 5, steps (a) and (b) are the normal ones involved in establishing an inverse square root of grain size, $\ell^{-1/2}$, dependence for the cleavage stress, σ_C, in the well-known Hall-Petch equation containing experimental constants, σ_{0C} and k_C

$$\sigma_C = \sigma_{0C} + k_C \ell^{-1/2} \tag{3}$$

It's the post-cracking step in Fig. 5(c) that provides a concentrated-stress-driven, high-rate performance of plastic work and accompanying production of localized heating which leads to a hot spot.[2] And, an important clue in the development of the pile-up avalanche model had been provided by the observation, indicated in Fig. 5(d), that hot spot sensitive materials were ones exhibiting discontinuous load drops in their deformation responses to drop-weight impact loading.[16]

A model description of such hot spot initiation led to the relationship, appropriate to energetic material properties, of

$$\Delta T \le \frac{k_S \ell^{1/2}}{16\pi} \left(\frac{2\upsilon}{c^* bK} \right)^{1/2} \tag{4}$$

In eq. (4), ΔT is the hot spot temperature rise, υ is the stress-dependent dislocation velocity, c^* is the specific heat at constant volume, b is the

dislocation Burgers (displacement) vector, K is the thermal conductivity, and $k_S = k_C/m$ in which m is a Taylor orientation factor. Upper limiting estimations of temperature rises and hot spot lifetimes were reported for a number of energetic and metallic materials under the condition of dislocations moving at the elastic shear wave speed.[17] Otherwise at normal impact loading conditions, the dislocation velocity follows an Arrhenius-type dependence expressed as

$$\upsilon = \upsilon_0 \exp\left(-\frac{G_0 - \int Ab\left[d\tau_{Th}\right]}{k_B T}\right) \qquad (5)$$

In eq. (5), υ_0 is the reference dislocation velocity, G_0 is the Gibbs free energy, A is the dislocation activation area under shear stress, τ_{Th}, and k_B is Boltzmann's constant. Equations (4) and (5) were combined with the conditions of $Ab = W/\tau_{Th}$ and $\tau_{Th}=H_{50}^{(1/n)}$, in the latter case in which H_{50} is the drop-weight height for 50% probability of initiation, to predict a greater temperature rise associated with deformation of larger crystals, as indicated by the proportionality relationship[18]

$$\log H_{50} \propto \left(\frac{nk_B T}{W_0}\right)\log\left(f\{\Delta T, T, ...\}\ell^{-1/2}\right)$$

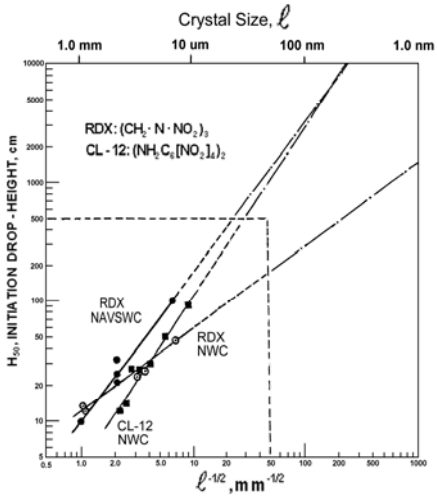

Fig. 6. Drop-weight height, H_{50}, dependence on $\ell^{-1/2}$, the reciprocal square root of crystal size.[18]

Fig. 6 shows application of the relationship to measurements made on RDX and CL-12 materials. In the figure, an increase in H_{50} by an approximate order of magnitude is achieved for RDX by a two-order of magnitude reduction in ℓ from ~ 1.0 mm to ~ 10 μm. Also, the originally reported ordinate and abscissa scales that are indicated now by the internal dashed boundary lines have been extended for possible indication of the results that may be achievable at nano-scale particle sizes.[19]

Further consideration has been given to evaluation of the hot spot temperature rise in terms of computing the work done by the individual dislocations as they speed away from a collapsed obstacle.[20] For the adiabatic case,

$$\Delta T = \left(\frac{\beta}{c * \ell}\right)\sum_{i=1}^{N} \tau_{i,eff}\upsilon_i \Delta t_i \qquad (6)$$

In eq. (6), $\beta \sim 1.0$ is a conversion factor for the transformation of plastic work to heat and $\tau_{i,eff}$ is the effective stress acting on the i^{th} dislocation with velocity, υ_i. Thus, the hot spot temperature is higher for reason both of a concentrated shear stress, $\tau_{i,eff}$, acting on each dislocation that travels at an enhanced υ_i also because of its locally concentrated higher stress, as determined by eq. (5). Figure 7 shows a comparison of pile-up avalanche results with corresponding thermal explosion temperatures.

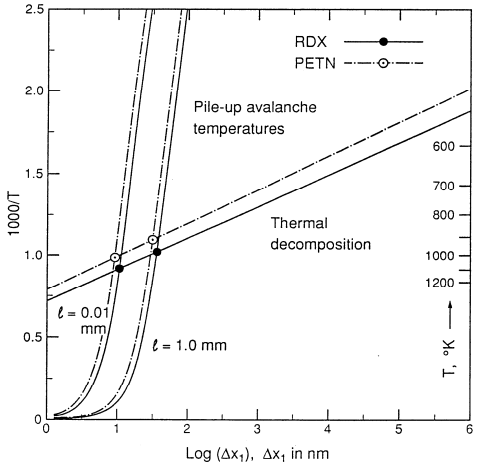

Fig. 7. Comparison of predicted RDX and PETN crystal initiations on pile-up avalanche and thermal explosion model calculations.

For the comparison purpose shown in Fig. 7, the thermal hot spot size has been taken equal to the separation of the two dislocations compressed at the tip of the pile-up.[18] On this basis, larger crystals are seen to undergo initiation at lower temperatures, consistent with the results in Fig. 6. And, PETN, because of its greater sensitivity to thermal explosion, is seen to be mechanically more sensitive than RDX, at the same crystal size.

Particle compaction

Beyond the individual crystal and particle effects described above, mechanically-induced compaction of energetic particle systems has been investigated under both static and dynamic loading conditions by making use of Hertzian hardness-type particle-to-particle contact theory, not unrelated to the results contained in Fig. 1.[20, 21] In the first case, a model for particle system densification was developed for a number of spherical ball propellants as shown below for the example in Fig. 8.

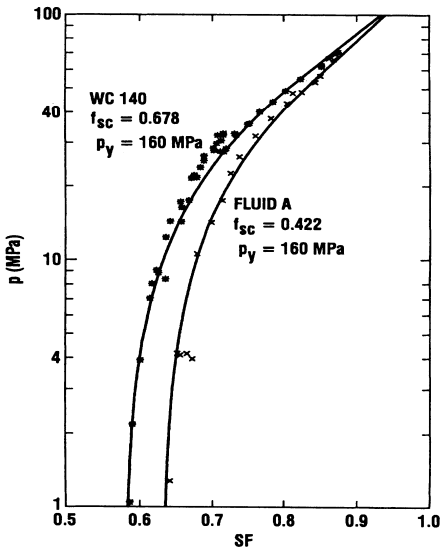

Fig. 8. Modeled description of pressure, p, vs. solid fraction, SF, for compaction results obtained on two solid ball propellant materials; P_y is the hardness-determined yield pressure and f_{SC} is the solid fraction arranged in a simple cubic lattice.[21]

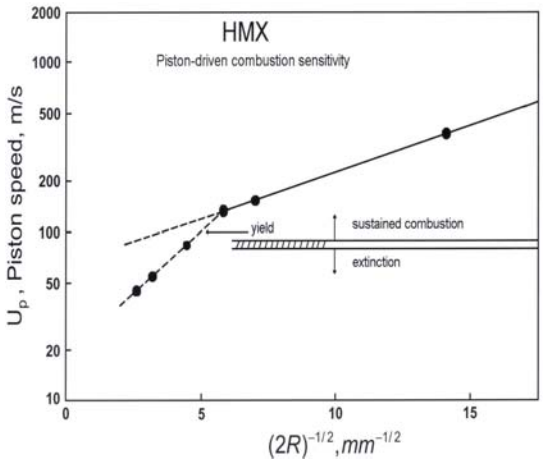

Fig. 9. Adaptation of modeled piston speed during compaction on the sustained combustion of spherical RDX particles of radius, R.[22,19]

In Fig. 9, that applies for the consideration of loading rate on granular compaction of an HMX particle system, a linear reciprocal particle diameter effect, $2R = \ell$, might be expected on the basis of the piston velocity being taken approximately proportional to the material strain rate; see eq. (5). And, the distinction is clearly demonstrated that sustained combustion required full intergranular yielding of the particle bed. Other compaction results obtained on HMX and related energetic material particles show additionally, even under quasi-static conditions, that particle fracturing occurred, particularly of larger sized particles fracturing more easily as indicted in Fig. 1 and eq. (3).[23] An expectation of strength dependence on the logarithm of strain rate was confirmed for compaction of an RDX porous bed.[24]

Most recently, investigation at greater burn rates within a high-pressure strand burner or diamond anvil cell of the deflagration-to-detonation transition (DDT), thus leading to shock considerations, has shown important discontinuous increases in burn rates both for HMX and RDX particle systems in association with solid-state phase transformations occurring at measured pressures of ~7 GPa.[25] The result relates to a pioneering report of the β-to-δ transformation in HMX being associated with the occurrence of

cracking below the surface of burning crystals and, thus, being of concern with respect to uncontrolled reactions.[26] A lesser effect occurred for smaller crystals, again in agreement with the type of size effect being described in the present report.

Shock results

The hot spot model for PBX's has been reviewed very recently with respect to obtaining a better understanding of energetic material properties under shock conditions, say, at pressures in the range $2.3 \leq P \leq 7.0$ GPa for an HMX-containing PBX 9501 formulation.[27] Such shock studies are generally conducted under pressures far above the stress levels causing plastic deformation and cracking of the energetic constituents even with incorporation of local stress enhancements from porosity and particle-to-particle contiguity concerns.[28] In this sense, the shock-type behaviors of energetic materials and their formulations are more complicated than those of reference inert metal and certain ionic materials, for example, as illustrated in the latter case by dynamic x-ray diffraction results obtained on an MgO crystal laser-shocked along the [100] direction to produce simple one-dimensional compression up to a strain of 0.046.[29]

Figure 10 shows a view of such laser-shocked complication for cracking occurring first in the orthorhombic phase and then followed by finer cracking in the cubic phase of an AP crystal.[30]

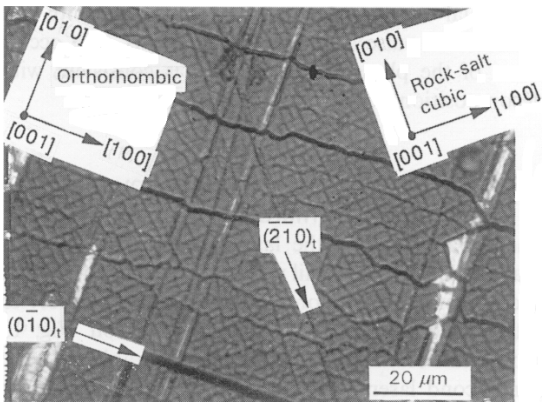

Fig. 10. [001] laser-shocked AP crystal.[30]

As identified in the scanning electron microscope (SEM) image in Figure 10, a striped array of relatively larger scale (0-10) and (-2-10) cracking occurred in the ambient temperature orthorhombic phase before {100} cracking, typical of the rocksalt crystal structure, occurred because of the pulsed-laser action. Chlorate decomposition was established via x-ray photoelectron spectroscopy (XPS) measurements, and sub-surface reaction sites were able to be identified in atomic force microscope (AFM) images. Beyond development of a dislocation reaction description for the observed cracking, a model-based explanation was given for the influence of the hydrostatic stress-state of the reacted dislocation-cracks on promoting hollow sub-surface decomposition sites that were observed in AFM images. The model description was associated with an earlier account of "more gentle" laser-induced melting and associated cracking observations made on an RDX crystal surface.[31]

Thus, in relation to drop-weight impact test results obtained at highest pressures of ≤ 1 GPa, as shown for the results in Fig. 6, significantly greater shock pressures, also above phase transformation levels, are associated with even pre-detonation results obtained on both energetic crystals and their material formulations.[27, 32, 33] Such a comparison is adapted in Fig. 11 from a study of particle size and crystal quality on shock initiation via Insensitive High-Explosive Gap Test (IHEGT) pressure measurements reported for two RDX/HTPB formulations.[34]

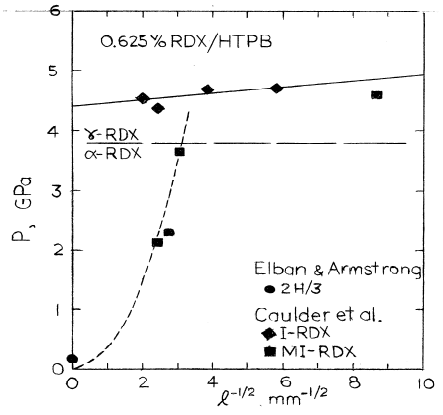

Fig. 11. P vs. $\ell^{-1/2}$ shock sensitivity measurements.

In Fig. 11, the 50% initiation pressures are shown for formulations incorporating differently sieved, essentially mono-modal, either insensitive RDX (I-RDX) or ultra-pure moderately insensitive (MI-RDX) particles. As evident, significantly different particle size effects were observed in the two cases, with the MI-RDX/HTPB formulations having particles exhibiting more surface defects and somewhat different particle morphologies. Examination of the two particle types by nuclear quadrapole resonance (NQR) spectroscopy revealed a much greater overall defect density within the MI-RDX material; and, the combination of overall internal and surface defect density in the MI-RDX material was concluded to account for the severally shown lower initiation pressures.

Very importantly, the shock sensitivity results in Fig. 11 provide for a comparison to be made at pressure levels spanning the range of static and dynamic values of concern in the present report. Such shock pressures are known to be connected to compressive stresses through the relationship

$$P = \sigma\left(\frac{1-\nu}{1-2\nu}\right) \qquad (7)$$

With $P \sim 2\sigma$ from eq. (7), and $\sigma \sim \sigma_H/3$, with σ_H taken as 24 MPa from Fig. 1, a value of P ~ 16 MPa is plotted near to the origin of the ordinate axis in Fig. 11 to approximate to the static hardness pressure for deformation of an RDX crystal. In turn, the MI-RDX shock sensitivity results are seen to span the range in pressure from an essentially static hardness pressure for plastic flow and much higher pressures, eventually rising above the α-to-γ transformation at ambient temperature. As mentioned above, near to the same pressure but at somewhat higher temperature, either α or γ transforms to β.[15]

The ultra-pure quality of the MI-RDX constituent suggests the possibility that the below-phase-transformation shock sensitivity results might be determined by generation of hot spots via the mechanism of dislocation pile-up avalanches. For this reason, eq. (4) has been adapted to provide the relationship shown graphically as

$$P = 2mB\left(\frac{c^* bK}{2}\right)\left(\frac{16\pi\Delta T}{k_S}\right)^2\left(\ell^{-1/2}\right)^2 \qquad (8)$$

In eq. (8), $P \sim 2m\tau \sim v/B \sim 0.38\ \ell^{-1}$ for assumed drag control of dislocation velocities at these high pressures and for which B is the drag coefficient. Thus, according to the present suggestion, the lower MI-RDX formulation may be initiated by dislocation pile-up avalanches occurring at the indicated sub-phase-transformation pressures.

Comparison can be made also with the pressure dependence on particle size shown for the shock sensitivity results above the phase transformation. The I-RDX results are fitted to

$$P = 43.4 + 0.065\ell^{-1/2} \qquad (9)$$

With $P \sim 2m\tau$, a value of $k_P \sim 0.048$ GPa.mm$^{1/2}$ is evaluated based on a previous estimation[17] of $k_S \sim 0.0077$ GPa.mm$^{1/2}$. Agreement with the experimental $k_P = 0.065$ GPa.mm$^{1/2}$ is surely fortuitous because order of magnitude agreement should be expected at best.

Conclusion

Energetic material hardness, drop-weight impact, particle compaction, combustion, and shock results are connected positively with dislocation mechanics and phase transformation behaviors.

References

1. Armstrong, R.W., and Elban, W.L., "Macro- to Nano-indentation Hardness Stress – Strain Aspects of Crystal Elastic/Plastic/Cracking Behaviors", *Exp. Mech.*, DOI 10.1007/s11340-009-9246-5, 2009.

2. Armstrong, R.W., Coffey, C.S., and Elban, W.L., "Adiabatic Heating at a Dislocation Pile-up Avalanche", *Acta Metall.*, Vol. 30, pp. 2111-2118, 1982.

3. Hammond, B.L., and Armstrong, R.W., "Recovered Elastic and Plastic Strains at Residual

Micro-indentations in an MgO Crystal", *Philos. Mag. Letts.*, Vol. 57, pp. 41-47, 1988.

4. Armstrong, R.W., and Elban, W.L., "Dislocations in Energetic Crystals", in *Dislocations in Solids*, edited by F.R.N. Nabarro and J.P. Hirth, Vol. 12, pp. 403-446, Elsevier B.V., Oxford, 2004.

5. Lucca, D.A., Klopfstein, M.J., Mejia, O.R., Rossettini, L., and DeLuca, L.T., "Investigation of Ammonium Perchlorate by Nanoindentation", *Mater. Sci. Tech.*, Vol. 22, pp. 396-401, 2006.

6. Elban, W.L., and Armstrong, R.W., "Plastic Anisotropy and Cracking at Hardness Impressions in Single Crystal Ammonium Perchlorate", *Acta Mater.*, Vol. 46, pp. 6041-6052, 1998.

7. Elban, W.L., Coyne, P.J., Jr., and Armstrong, R.W., "Mechanical Property Determination of Single Crystal Ammonium Perchlorate", unpublished results, 1998.

8. Armstrong, R.W., "Dislocation Pile-ups: From {110} Cracking in MgO to Model Strength Evaluations", *Mater. Sci. Eng. A,* Vol. 409, pp. 24-31, 2005.

9. Elban, W.L., and Armstrong, R.W., "Microhardness Study of RDX to Assess Localized Deformation and Its Role in Hot Spot Formation", in *Proceedings of the 7th Symposium (International) on Detonation*, pp. 976-985, Annapolis, MD, June, 1981.

10. Armstrong, R.W., and Raghuram, A.C., "Anisotropy of Microhardness in Crystals", in *The Science of Hardness Testing and Its Research Applications*, edited by J.H. Westbrook and H. Conrad, pp. 174-186, Amer. Soc. Metals, Metals Park, OH, 1973.

11. Hagan, J.T., and Chaudhri, M.M., "Fracture Surface Energies of High Explosives PETN and RDX", *J. Mater. Sci.*, Vol. 12, pp. 1055-1058, 1977.

12. Yoo, K.-C., Rosemeier, R.G., Elban, W.L., and Armstrong, R.W., "X-ray Topography Evidence for Energy Dissipation at Indentation Cracks in MgO Crystals", *J. Mater. Sci. Letts.*, Vol. 3, pp. 560-562, 1984.

13. Armstrong, R.W., and Elban, W.L., "Cracking at Micro-hardness Indentations in RDX Explosive and MgO Single Crystals", *Mater. Sci. Eng.*, Vol. A111, pp. 35-43, 1989.

14. Cawkwell, M.J., Sewell, T.D., Zheng, L., and Thompson, D.L., "Shock-induced Shear Bands in an Energetic Molecular Crystal: Application of Shock-front Absorbing Boundary Conditions to Molecular Dynamics Simulations", *Phys. Rev. B*, 78, 014107, 2008; see referenced Cawkwell, M.J., Sewell, T.D., Ramos, K.J., and Hooks, D.E., "Homogeneous Dislocation Nucleation and Anomalous Hardening in RDX", unpublished, 2007.

15. Russell, T.P., Miller, P.J., Piermarini, G.J., and Block, S., "Pressure/Temperature/Reaction Phase Diagrams for Several Nitramine Compounds", in *Structure and Properties of Energetic Materials*, edited by D.H. Liebenberg, R.W. Armstrong, and J.J. Gilman, Vol. 296, pp. 199-213, Mater. Res. Soc., Pittsburgh, PA, 1993.

16. Heavens, S.N., and Field, J.E., "The Ignition of a Thin Layer of Explosive by Impact", *Proc. Roy. Soc. Lond.*, Ser. A, Vol. 338, pp. 77-93, 1974.

17. Armstrong, R.W., and Elban, W.L., "Temperature Rise at a Dislocation Pile-up Avalanche", *Mater. Sci. Eng.*, Vol. A122, pp. L1-L3, 1989.

18. Armstrong, R.W., Coffey, C.S., DeVost, V.F., and Elban, W.L., "Crystal Size Dependence for Impact Initiation of Cyclotrimethylenetrinitramine Explosive", *J. Appl. Phys.*, Vol. 68, pp. 979-984, 1990.

19. Armstrong, R.W., "Dual Advantages of Ultra Fine Crystal-sized Energetic/Reactive Material Formulations", in *Advancements in Energetic Materials and Chemical Propulsion*, edited by K.K. Kuo and J. de Dios Rivera, pp. 331-341, Begell House, Inc., N.Y., 2007.

20. Grise, W.R., "Hot Spots from Dislocation Pile-up Avalanches", in *Multifunctional Energetic Materials*, edited by N.N. Thadhani, R.W. Armstrong, A.E. Gash, and W.H. Wilson, Vol. 896, pp. 177-189, Mater. Res. Soc., Warrendale, PA, 2006.

21. Jacobs, S.J., Sandusky, H.W., and Elban, W.L., "Quasi-static Compaction of Porous Beds. I. Modeling Ball Powder Experiments with Deformed Spheres in a Regular Lattice", *Powder Tech.*, Vol. 89, pp. 209-217, 1996.

22. Gonthier, K.A., "Modeling and Analysis of Reactive Compaction for Granular Energetic Solids", *J. Appl. Phys.*, Vol. 95, 3482-3488, 2004.

23. Elban, W.L, and Chiarito, M.A., "Quasi-static Compaction Study of Coarse RDX Explosive", *Powder Tech.*, Vol. 46, pp. 181-193, 1986.

24. Coyne, P.J., Jr., Elban, W.L., and Chiarito, "The Strain Rate Behavior of Coarse HMX Porous Bed Compaction", in *Proceedings 8th Symposium (International) on Detonation*, pp. 645-657, Albuquerque, NM, July, 1985; NSWC MP 86-194.

25. Zaug, J.M., Young, C.E., Long, G.T., Maienschein, J.L., Glascoe, E.A., Hansen, D.W., Wardell, J.F., Black, C.K., and Sykora, G.B., "Deflagration Rates of Secondary Explosives under Static MPa – GPa Conditions", in *Shock Compression of Condensed Matter – 2009*, edited by M.L. Elert, W.T. Buttler, M.D. Furnish, W.W. Anderson, and W.G. Proud, CP1195, Part One, pp. 420-423, Amer. Phys. Soc., Melville, N.Y., 2009.

26. Karpowicz, R.J., and Brill, T.B., "The β→δ Transformation of HMX: Its Thermal Analysis and Relationship to Propellants", *AIAA J.*, Vol. 20, pp. 1586-1591, 1982.

27. Menikoff, R., "On Beyond the Standard Model for High Explosives: Challenges & Obstacles to Surmount", in *Shock Compression of Condensed Matter – 2009*, edited by M.L. Elert, W.T. Buttler, M.D. Furnish, W.W. Anderson, and W.G. Proud, CP1195, Part One, pp. 18-25, Amer. Inst. Phys., Melville, N.Y., 2009.

28. Armstrong, R.W., "Dislocation Mechanics Aspects of Energetic Material Composites", *Rev. Adv. Mater. Sci.*, Vol. 19, pp. 13-40, 2009.

29. Hironaka, Y., Shigemori, K., Kadono, T., Fugioka, S., Tanabe, M., Shiroshita, A., Ozaki, N., Miyanishi, K., Kondo, T., Otani, K., Sakaiya, T., and Shimizu, K., "Wide Angle X-ray Diffraction for Shocked Periclase", in *Shock Compression of Condensed Matter – 2009*, edited by M.L. Elert, W.T. Buttler, M.D. Furnish, W.W. Anderson and W.G. Proud, CP1195, Part One, pp. 607-610, Amer. Inst. Phys., Melville, N.Y., 2009.

30. Ramaswamy, A.L., Shin, H., Armstrong, R.W., Lee, C.H., and Sharma, J., "Nanosecond and Picosecond Laser-induced Cracking and Ignition of Single Crystals of Ammonium Perchlorate", *J. Mater. Sci.*, Vol. 31, 6035-6042, 1996.

31. Armstrong, R.W., Ramaswamy, A.L., and Field, J.E., "Thermomechanical Influences on the Combustion of RDX Crystals", in *ONR/SNPE/ ONERA Workshop on Explosive and Propellant Combustion Mechanisms*, edited by R.W. Armstrong, ONREUR Report 91-02-w, pp. 168-176, U.S. Office of Naval Research, European Office, London, U.K., 1991.

32. Walley, S.M., Field, J.E., and Greenway, M.W., "Crystal Sensitivities of Energetic Materials", *Mater. Sci. Tech.* Vol., 22, 402-413, 2006.

33. Fanget, A., Nadot, C., Dragon, A., and Jeulin, D., "Mesoscopic to Macroscopic Behavior of Particulate Composites: Experimental and Numerical Aspects", in *Shock Compression of Condensed Matter – 2009*, edited by M.L. Elert, W.T. Buttler, M.D. Furnish, W.W. Anderson, and W.G. Proud, CP1195, Part One, pp. 343-348, Amer. Inst. Phys., Melville, N.Y., 2009.

34. Caulder, S.M., Miller, P.J., Gibson, K.D., and Kelley, J.M., "Effect of Particle Size and Crystal Quality on the Critical Shock Initiation Pressures of RDX/HTPB Formulations", in *Proceedings of the 13th International Symposium on Detonation*, pp. 656-661, Norfolk, VA, July, 2006.